Characterization of iron oxides-based red pigments in the ancient Gaya region, South Korea

Dong Hyeok Moon[1] · Na Ra Lee[1] · Woo Rim Han[2] · So Jin Kim[1] · Young Rang Uhm[3]

Abstract

The characteristics of red pigments of the Gaya cultural circles, the ancient federation kingdom in the southern part of the Korean Peninsula, have been investigated using multiple analyses (SEM–EDS, XRD, Raman and Mössbauer spectroscopy). In results, reddish ochre- and pure hematite-based pigments were distinguished. In addition, as the redness of the pigment increased, the proportion of well crystalline and magnetically ordered α-Fe_2O_3 phase also increased, whereas the amorphous and superparamagnetic Fe_2O_3 phase were decreased. These results indicate that the ancient Gaya people produced various red pigments according to their use by thermal treatment of reddish ochre and high-purity iron compounds.

Keywords Ancient pigment · Red ochre · Hematite · Phase analysis · Iron-oxides characterization · Gaya cultural circles

Introduction

Since the prehistoric era, humans have used mineral-based coloring materials (pigments) in paintings, makeup, architectural structures, sculptures, and the ceramic surfaces for the purposes of coloring, decoration, protection, ritual, and ceremonial meaning [1–5]. Among all the natural minerals, iron oxide-based reddish materials, is the most widely used as a pigment in human history around the world [4–9]. In general, two major groups of iron-oxides predominate in natural ochre, generated from the weathering environment, such as Fe^{3+}-oxides and -oxyhydroxides, simply termed as "iron oxides" in this paper. Moreover, recent scientific analysis reveals that Neanderthals, who were active before modern humans, also used iron oxide-based red ochre as pigments [10–12]. It is because various earthy pigments of yellow, red and brown, commonly called ocher, were generally abundant

in surface deposits, so that they were relatively cheap and easily available. Furthermore, the formation of the reddish mineral hematite, well crystalline α-Fe_2O_3 with weak ferromagnetic properties, in ochre by thermal treatment were common in human history, a process was already known in antiquity [13]. In addition, recent literatures explain the effect of thermal treatment on color changes, along with the particle size, crystallinity, purity, and magnetic property of hematite in iron oxides-based raw materials for ancient red pigments [13–15].

In Korea, such iron oxides-based red pigments are also found in archaeological sites and cultural heritages throughout all historical periods. In particular, red paint-ceremony, held in the tumulus, is closely related to social ideas and faith of the ancient Kingdoms, established after the Iron Age. In addition, these traces are considered as ritual action of the ruling class accompanied by an expert group, such as shamans and/or Buddhist monks [4, 16].

Recently, excavation of red pigments in ancient tombs of the Gaya cultural circles, the ancient federation kingdom in the southern region of the Korean Peninsula (1st–6th centuries AD), has been reported; which excavated in various forms, such as stored in vessels, painted on the walls of stone chambers, murals, corpses, and artifacts. Elemental and mineral phase analyses have previously been used to identifications of their raw materials and combinations, resulted in iron oxide-based and cinnabar-based red pigments were distinguished [16–18]. However, in the case

✉ Dong Hyeok Moon
moondh@korea.kr

Young Rang Uhm
uyrang@kaeri.re.kr

[1] Conservation Science Division, National Research Institute of Cultural Heritage, Daejeon 34122, Republic of Korea

[2] Gaya National Research Institute of Cultural Heritage, Changwon 51430, Republic of Korea

[3] HANARO Utilization Division, Korea Atomic Energy Research Institute, Daejeon 34057, Republic of Korea

of iron oxides-based pigments, they have been referred to as simply "high-purity and/or low-purity iron oxide pigments", despite the extraordinary discovery of pulverized pigment, as well as different fragments of red pigment and a significant number of red-painted archaeological remains at these regions. Because they have never been considered for specific iron oxides phase analysis; their iron-oxides components are often characterized by small crystal size, significantly low concentrations, high foreign element substitutions, and close intergrowths with other associated fine grained mineral particles. With regard to these factors, ^{57}Fe Mössbauer spectroscopy contributes to distinguish and identify individual structural forms, amorphous and superparamagnetic nanostructured iron oxides particles, to analyze magnetic behavior caused by their formation mechanism. Therefore, in combination with chemical and physical methods, ^{57}Fe Mössbauer parameters are can supports to more valuable information for identification and characterization of iron-bearing minerals in natural materials and its artefacts, which are difficult to distinguish by phase analyzes that have been generally performed [8, 19–24].

In this context, this study will identify the variety of mineral composition (especially magnetic characteristics of each iron-oxides phases) used as red pigments in four ancient tombs of three renowned Gaya sites in Haman, Gimhae and Hapcheon in Gyeongsangnam-do Province, South Korea (Fig. 1). Furthermore, they were assessed to determine whether the natural minerals were used, or if they were transformed into artificial iron compounds by pre-treatment.

Experimental

## Archaeological outline and sample description

Four red pigment samples for each type from the ancient tombs of Gaya cultural circles of these three archaeological regions were considered for analysis: Haman, Gimhae, and Hapcheon (Fig. 1 and Table 1).

Gaya is the ancient federation kingdom in the southern region of the Korean Peninsula (1st–sixth century AD). Among the three regions where the tombs are located in this investigation, Gimhae region was the seat of "Garak-guk", the leader of the Gaya federation. In addition, Haman and Hapcheon were the provenances of small allies such as "Aragaya" and "Daraguk", respectively. Moreover, their archaeological remains excavated from ancient tombs in these regions reflect the powerful authority of the ruling class and the fact that each small allies grew up on a similar cultural basis.

As described in Table 1, red pigments were preserved in different status in each tumulus, and specimens for analysis were collected in powder form. For specimen analyses, the collected powders were directly used, and additional grinding was performed only for structural analysis.

Instrumentation and measurements

The raw powders of each pigment were observed using a microscope (Axio Imager A2, Zeiss, Germany), and the
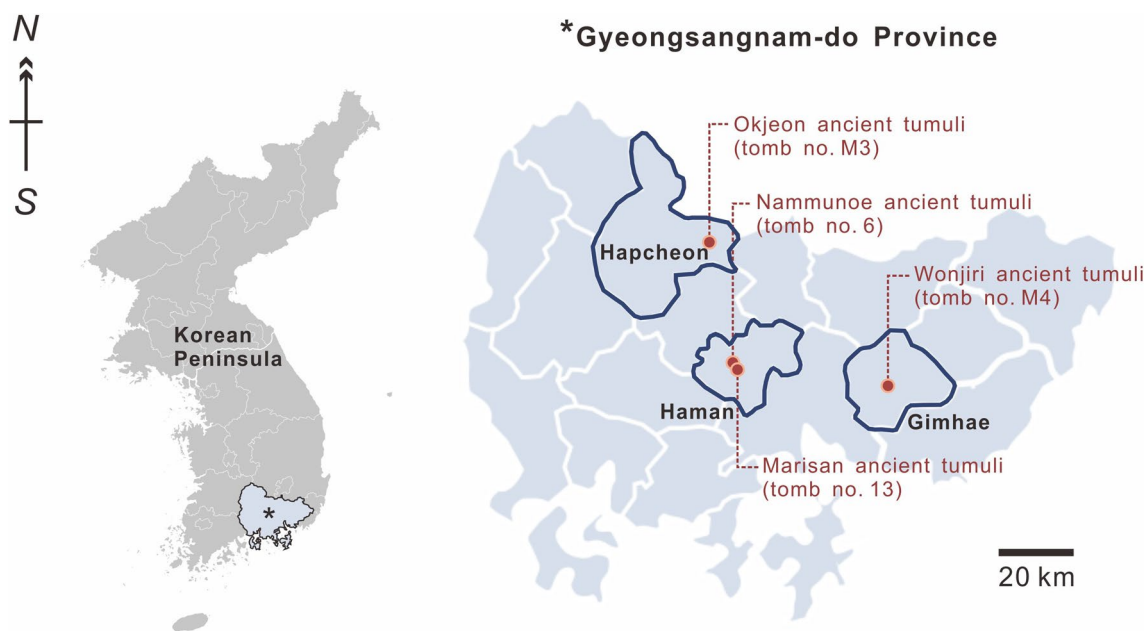
Fig. 1 Location and tomb numbers of the pigment collection sites

Table 1 The collection site, description, Lab CIE color coordinates of the pigment samples

Sample	Collection site	Description of sample	L^*–a^*–b^*	Visualized hue
Type 1	Ancient tomb no. 6 in the Nammunoe tumuli, Haman	Traces of the reddish-orange pigment, remaining on the mound wall	60.3–18.8–30.3	
Type 2	Ancient tomb no. 13 in the Marisan tumuli, Haman	Fine reddish-brown powder, painted on the rock fragment brick	48.8–9.9–15	
Type 3	Ancient tomb no. M4 in the Wonjiri tumuli, Gimhae	Block of red pigment paste, stored in a vessel	44.1–28.6–26.1	
Type 4	Ancient tomb no. M3 in the Okjeon tumuli, Hapcheon	Finely ground red pigment (no information on storage conditions)	39.9–29.5–20.2	

elemental distribution of each particle was analyzed using a scanning electron microscope with energy dispersive X-ray spectroscopy (SEM–EDS, MIRA3-LMH, Tescan, Czech). Chromaticity determinations were performed by Color Spectrophotometer (S60, X-rite co., USA), and recorded based on the L*a*b* space model proposed by Commission International d'Eclairge (CIE); L* is measure of lightness, a* redness, and b* yellowness.

X-ray diffraction (XRD), Raman and Mössbauer spectroscopy were performed to identify the mineral composition and magnetic properties of the samples. The XRD diffractograms were recorded using a Cu-Kα diffractometer (Empyrean, Malvern Panalytical, BK), which scanned in the range of 5°–60° 2θ at 45 kV and 40 mA with a scanning interval of 0.02° 2θ. Micro-Raman spectra were obtained using an XperRam F2.8 (Nanobase, Republic of Korea), with ×40 focused BX41M-LED microscope (Olympus, Japan). Laser wavelength of 473 nm (2300 gr/mm) was used for excitation. Mössbauer spectra were recorded using ^{57}Co (60 mCi) that was diffused in Rh as a γ-ray source at 295 K. Isomer shifts were referred to as α-Fe at room temperature. Subsequently, the obtained spectra were fitted to Lorentzian shapes and decomposed into quadrupole doublets and sextets using a MossWinn 4.0i program.

## Analytical results

Morphology and elemental distribution

The detailed shape and color of the particles in each sample were observed by microscope, SEM, and color spectrophotometer as shown in Fig. 2 and Table 1. Two painting layer samples with the orange and reddish-brown color (type 1 and type 2, respectively), consist inequigranular particles. Overall, the particles are characterized by the coexistence of micro-sized polyhedric particles with sharp borders and platy crystal, and nano-sized dispersed particles that covering the surface of micro-particles. In addition, black colored single particles are partially observed in type 1. As for the red pigment paste sample (type 3), medium to high rounded polyhedron shaped nano-particles were mainly observed, and light-colored coarse-grained mineral particles appear to be mixed. The sample type 4, with the highest redness, has only nano-sized irregular polyhedral particles with rounded edge. Moreover, these nanoparticles of the sample type 4 have clearly higher dimensions, sphericity and rounding than those of the sample type 3.

The chemical composition of the particles in each sample were characterized by SEM–EDS. In addition, the EDS mapping of the elements was carried out as shown in Fig. 3, with attention to the indicator elements of the iron oxides and ochres (i.e., iron, silicon and aluminum). The elemental distribution of type 1 shows that iron, results confined to particles of small dimensions compared to silicon and aluminum. In addition, the iron-containing particles are observed in a dispersed pattern on the silicate particles without forming large-sized aggregates, and some Fe-rich single particles are rarely confirmed. In the type 2, most of the iron distribution patterns are similar to type 1, while some particles are observed in an overlapped with silicon
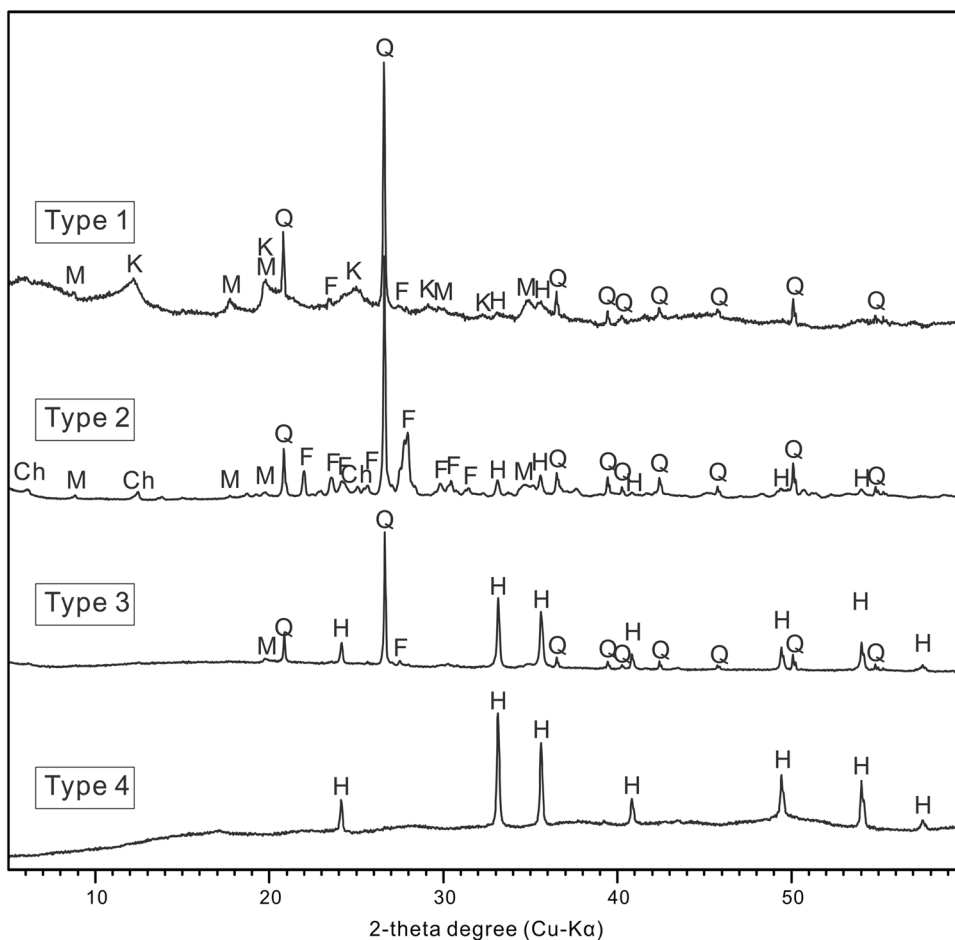
Fig. 2 Microscopic and SEM images of each type of pigments for **a**, **b** Type 1, **c**, **d** Type 2, **e**, **f** Type 3, and **g**, **h** Type 4
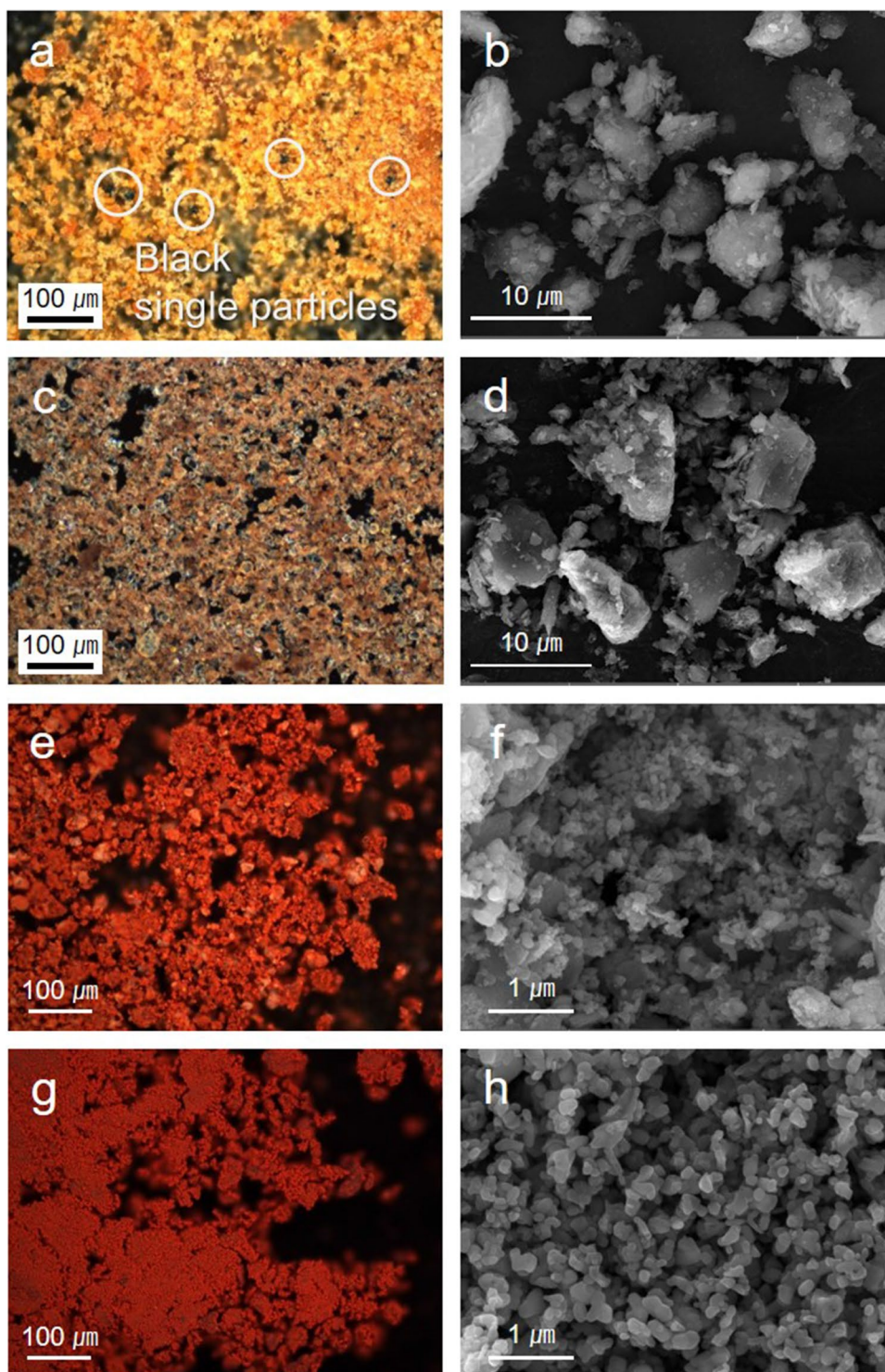
Fig. 3 SEM–EDS elemental distribution maps of the pigment samples for **a** Type 1, **b** Type 2, **c** Type 3, and **d** Type 4
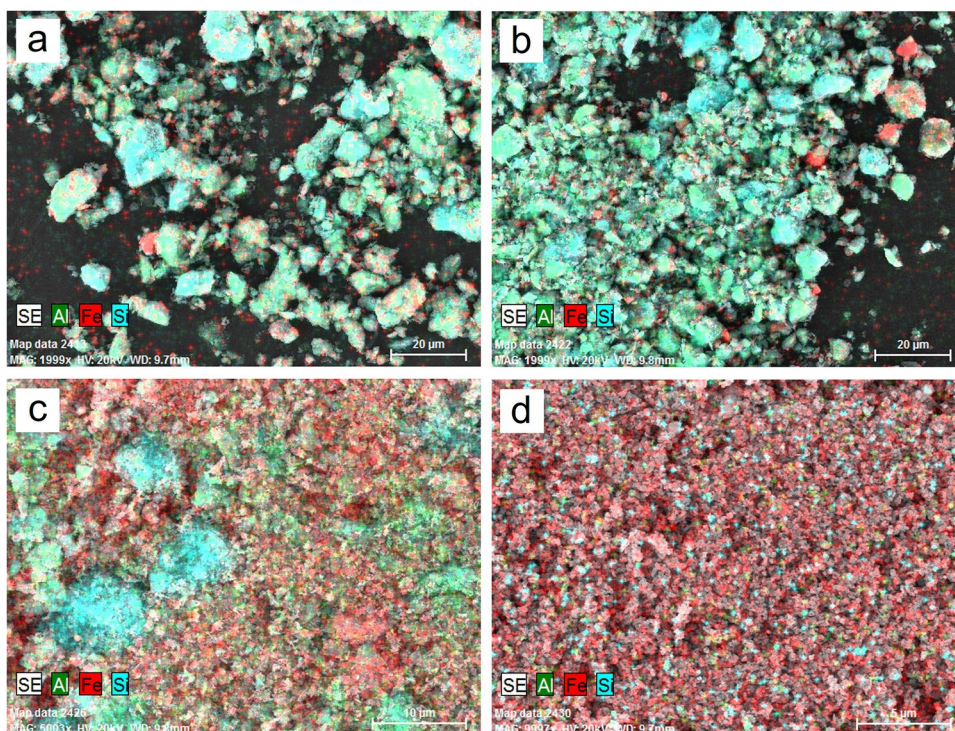
Fig. 4 X-ray diffraction patterns of the pigment samples (Ch: chlorite, F: feldspar, H: hematite, K: kaolin, M: mica, Q: quartz)

and aluminum. In contrast, the EDS elemental mapping of the type 3 and type 4 revealed aggregates of the iron oxides. The type 3 is characterized by the mixture of some silicate and alumino-silicate particles, while the type 4 is the identified as compound of pure iron oxides.

## Mineral phase identification: bulk powder and reddish particles

The result of bulk powder XRD for each specimen are illustrated in Fig. 4. The type 1 shows as major crystalline phases in the soil, such as quartz, feldspar, mica group minerals, and kaolin. In addition, very weak diffraction patterns of (104) and (110) peaks of hematite are recorded near the 33 and 35.6° 2-theta area; as well as the weak (311) peak of magnetite overlaps with the (110) peak of hematite, which is

detected with relatively higher intensity. The diffractogram of type 2 shows the presence of quartz, feldspar, chlorite group minerals, mica group minerals, and more crystalline phase of hematite than that of type 1. In the type 3, quartz and hematite, with a predominance of hematite, are the main mineral phases with weak traces of feldspar and mica. Finally, XRD analysis of type 4 shows the presence of pure hematite.

Figure 5 presents Raman spectra of the red-colored particles in each sample. As for the type 1, characteristic resonant peaks of hematite were not detected, while broad and weak hematite peaks were detected at 222 cm^{-1}, 292 cm^{-1}, 412 cm^{-1} and 610 cm^{-1} in the type 2. In addition, for these two samples, the characteristic Raman spectral peaks of quartz appeared at 463 cm^{-1} and 205 cm^{-1}, 356 cm^{-1}, 463 cm^{-1}, respectively. The Raman spectra of reddish particle in the type 3 and type 4 appear only sharp hematite peak at 223 cm^{-1}, 288 cm^{-1}, 408 cm^{-1}, and 602 cm^{-1} (cf. for the type 4, another hematite peak at 497 cm^{-1} was observed).
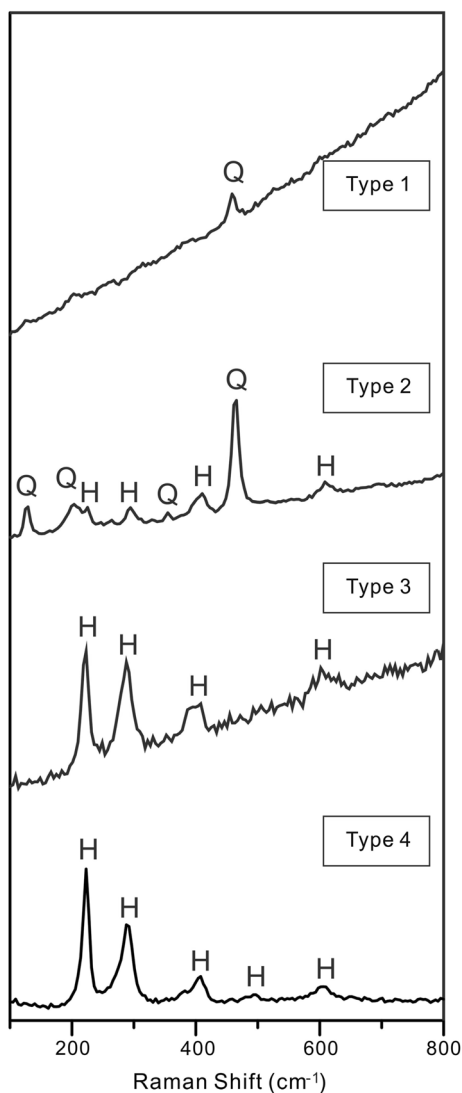
Fig. 5 Raman spectra of reddish particles in the pigment samples (H: hematite, Q: quartz)
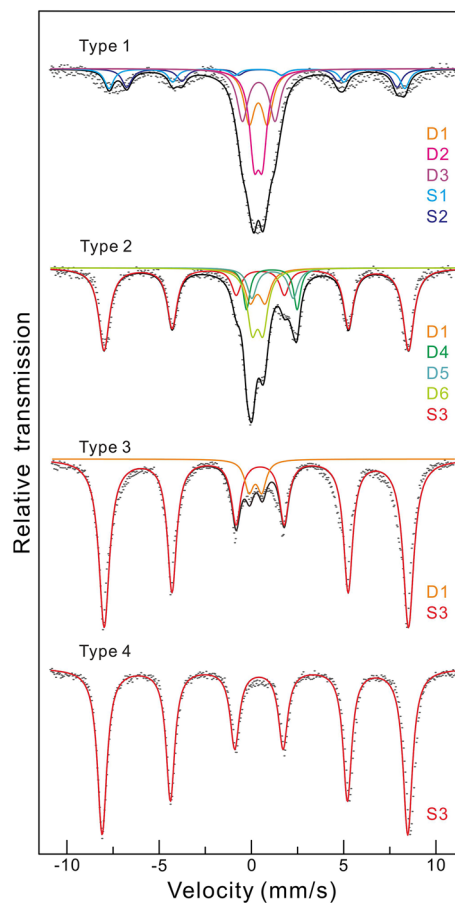
Fig. 6 Mössbauer spectra of the pigment samples at 295 K

Table 2 Mössbauer parameters of the pigment samples at 295 K (δ = isomer shift, E_Q = electric quadrupole splitting, H_{hf} = magnetic hyperfine field)

Sample	Spectra	Δ (mm/s)	E_Q (mm/s)	H_{hf} (kOe)	Area (%)	Iron compound phase (assigned iron-bearing mineral)
Type 1	D1	0.35	0.98	–	21.4	Fe^{3+} (superparamagnetic Fe_2O_3)
	D2	0.35	0.45	–	28.6	Fe^{3+} (kaolin)
	D3	0.38	1.77	–	21.4	Fe^{3+} (clay mineral)
	S1	0.31	−0.07	500.00	14.3	Fe_3O_4 (magnetite-A site)
	S2	0.50	0.10	456.43	14.3	Fe_3O_4 (magnetite-B site)
Type 2	D1	0.31	0.81	–	10.5	Fe^{3+} (superparamagnetic Fe_2O_3)
	D4	1.09	2.75	–	8.8	Fe^{2+} (clinochlore)
	D5	1.13	2.25	–	8.8	Fe^{2+} (clinochlore)
	D6	0.31	0.59	–	17.6	Fe^{3+} (clinochlore)
	S3	0.35	−0.22	514.20	54.3	$\alpha\text{-}Fe_2O_3$ (hematite)
Type 3	D1	0.25	0.69	–	6.2	Fe^{3+} (superparamagnetic Fe_2O_3)
	S3	0.37	−0.20	512.43	93.8	$\alpha\text{-}Fe_2O_3$ (hematite)
Type 4	S3	0.37	−0.22	518.20	100	$\alpha\text{-}Fe_2O_3$ (hematite)

Characterization of iron compounds: Mössbauer spectroscopy

Further details on the iron compounds were obtained from Mössbauer spectra collected at room temperature (295 K) as shown in Fig. 6, and their Mössbauer parameters were summarized in Table 2. The Mössbauer spectra each consist of several subspectra that are overlapped on each other showing that at least two iron containing phases are present.

The decomposed spectrum of type 1 shows a superparamagnetic behavior, which dominated by three quadrupole doublet; whose parameters are consistent with superparamagnetic Fe^{3+} of iron oxides (D1) and Fe^{3+} in the phyllosilicate structure of fine clay minerals (D2 and D3) [21–36]. In addition, two sextets of hyperfine magnetic splitting were also contained, which associated with magnetite (S1 and S2) [21–24]. The Mössbauer spectrum of type 2 appears as four distinct doublets (D1, D4, D5, and D6) and a single magnetically split sextet (S3). The computed parameters indicate that for each components, D1 corresponds to Fe^{3+} in superparamagnetic iron oxides, and D4, D5, and D6 assigned to paramagnetic Fe^{2+} and Fe^{3+} in chlorite group minerals (clinochlore), respectively [35, 36]. Moreover, S3 is identified as magnetic phase of hematite [21, 27, 29]. In the hematite rich and deep reddish-brown pigments, type 3, the Mössbauer spectrum appears as the sum of almost fully sextet with relatively sharp lines, attributable to weakly ferromagnetic hematite, and some trace of a central doublet which is associated to paramagnetic iron oxides [21–31]. For the Mössbauer data in type 4, the spectrum consists of a single sextet with sharp lines, and the parameters are fitting with those expected for weakly ferromagnetic hematite [21, 27, 29].

Discussion on pigment preparation

The renewed multi-analysis investigation on four typical red pigments allowed us to improve previous inferences on iron oxides-based painting materials in Gaya cultural circles [16–18]. Taking into account micromorphological and chemical evidence, XRD, Raman, and Mössbauer spectroscopic techniques, we are able to further optimize the interpretation of iron oxides composition on various types of red pigment. Moreover, these analyzed results propose how each type of iron-oxides based red pigment were manufactured.

The elemental distribution and mineral phase of red particles in the type 1 and type 2 showed that silicate minerals, such as quartz, alumino-silicate and phyllosilicate (including clay minerals), are the main component. Such abundance of silicates can also be explained by a lower quantity and dispersed iron oxide distribution. These analysis results indicate that the type 1 and type 2 were prepared using natural soil as a raw material. However, these two ochre-based pigments involved remarkably different magnetic behavior of iron oxides. It is clearly indicated that the spectral area of sextet relative to the central doublet appear higher proportion in the brown ochre (type 2) compared to the orange ochre (type 1). These results may correspond to an ultrafine-sized and poorly crystallized hematite and/or Fe^{3+} ions hidden by the high levels of silicate mineral in reddish particles in the type 1 [7, 21–37]. In contrast, the dominant sextet in the type 2, a fully magnetically split Mössbauer spectra at room temperature, represents a magnetically ordered component, possibly with weakly ferromagnetic properties, and indicating that well-crystalline hematite particles [23, 24, 26, 29, 38]. In addition, we note that the sextets in type 1 is assigned to magnetite, which is observed as black particles in Fig. 2 and iron rich single-domain particle in Fig. 3. The presence of such single-domain sized magnetite indicates

that the type 1 used natural red ochre, due to this kind of mineral particles are usually inherited from the parent rocks, and/or occur under soil-forming conditions [39–41]. Furthermore, it is known to undergo the phase transition to hematite after heat treatment [42, 43]. Therefore, weakly ferromagnetic hematite in the type 2 indicating that sintering had taken place by thermal process [20, 26]. In addition, the higher ratio of Fe^{3+} than Fe^{2+} among the doublets assigned to chlorite group minerals (clinochlore) can also be interpreted as a result of heat treatment in an oxidized atmosphere [36]. These changes in the Mössbauer spectra reflect various phases of decomposition and transformation of the iron oxides.

In contrast to the above ocher-based pigments, the chemical and mineral composition of the type 3 and type 4 are composed of nearly pure hematite. It suggests the possibility that they were manufactured using high-grade massive iron ore or iron-containing materials rather than directly use of natural reddish ocher. In addition, more numerous and sharper shaped peaks in XRD diffractograms and Raman spectra of the samples type 3 and type 4, than those of two ochre-based pigments, correlate with the higher crystallinity of hematite [14, 42–45]. Moreover, we investigated the rounded polyhedron morphology of the hematite nano-particles, and their weak ferromagnetic properties in the room temperature Mössbauer spectra as shown in Figs. 2, 6. These results indicate that these two hematite-based pigments are synthetic painting materials which were thermally treated on purpose. In human history, this type of pigment is rarely reported before development of artificial ingredients of iron oxides, called Mars colours, nineteenth century [6–8, 14].

It is interesting comparing these two hematite-based pigments since they presented a huge variation in particle size and impurities, but the similar shade. The identified mineral composition show that they have been processed from a similar raw material with a high purity of iron components. However, their hematite characteristics indicate that the type 4 was calcined at a higher temperature than type 3, due to former has higher diameter, more rounded particles, and the larger spectral area of sextet related to weakly ferromagnetic properties than those of latter. In addition, another difference identified in the analysis results are the mix of small amount of soil as an extender to augment their volume and weight in the type 3. Considering sample description in Table 1, the two hematitic pigments, type 3 and type 4, were stored in the vessels, and has been identified as a block of red paste and a finely ground red pigment, respectively; in contrast to the two ochre-based pigments (type 1 and type 2) were discovered as painted status. Therefore, we can estimate that they have been stored as powder phase after manufactured by

their own processes. Such storage in powder form of hematite can be assumed to preparation for future needs rather than a one-time storage for immediate use [7].

A detailed study of the thermally induced synthesis of hematite and its temperature tracking is an extensive project in itself. Because the experimental results can be flexibly varied depending on the starting raw material, processing method, firing environment, and many other parameters [13–15, 20, 26, 27, 42, 43, 46]. Moreover, there is no documentary evidence on high-purity iron materials and additives. Thus, here we have paid attention to those aspects of the morphology, grain size, and magnetic behaviors that are related to hematite crystallinity by thermal treatment.

As is well-known common knowledge, although iron oxides are extremely abundant in the surface soil [47], so far not one of such oxides is suitable for phase analysis as chromophores. Because they are composed of poorly crystalline iron oxides, including amorphous phases and ferrihydrite [9, 48]. Moreover, iron oxides formed in naturally weathered soils consist of less crystalline phases due to a presence of inhibitors of crystallization, especially silica species and organic matter, and hence their color strength is insufficient. Therefore, as low as a few percent of well-crystalline hematite admixtures change the hue of yellowish ochre to brownish or reddish as shown in Table 1 and Fig. 2, because the color strength of hematite is greater than that of amorphous phase of iron oxides with poor crystallinity [7, 8, 15].

In this regard, our results confirm that successful contribution of the characteristic information towards the magnetic behavior of each iron oxides by Mössbauer spectroscopy; which can be a powerful tool for the identification and characterization of iron-bearing minerals in combination with chemical and physical methods. Consequently, multiple-analyzing data in this study are indicate that the color distribution characteristic of the iron oxides contained red painting materials are affected by their purity and crystallinity of hematitic iron oxides. It is clearly show that the hematite-based pigments have higher redness (a*) compared to ochre-based pigments. In addition, a significant decrease in brightness (L*) is observed as the proportion of well crystalline hematite increases in iron oxides-based pigments. Finally, considering our whole data set of four types of samples, it can be explained that the ancient Gaya people made use of these characteristics of iron oxides, and produced, stored, and used various types of iron oxide-based red pigments for each purpose (i.e., such as natural red ochre, thermally induced red ochre, pure hematitic pigment and its mixed paste with extender materials).

Conclusions

In present study, it has been demonstrated that the raw materials and process of the four characteristic iron oxides-based red pigments in the ancient Gaya cultural circles. The analyzing results using multi-characterization techniques (SEM–EDS, XRD, Raman and Mössbauer spectroscopy), indicate that the natural red ochre, thermally induced red ochre, and hematite-based materials (including heat-treated pure synthetic hematite powder, and extender mixed paste) were used as pigment preparation. Moreover, the color distribution characteristics of iron oxides-based red pigments are affected by an increase in redness (a^*) and a decrease in lightness (L^*), as increase of the concentration, crystallinity, and weakly ferromagnetic properties of hematitic iron oxides by thermal process. These results suggest that the ancient Gaya people produced various types of iron oxides-based pigments according to purpose, by selective application of raw materials and thermal process.

A method for detailed identification of iron oxides-based pigments was successfully improved using the Mössbauer spectroscopy: this tool may be used in the future in the analysis of iron compound-based painting materials, with the aim of uniquely identifying the ancient iron oxides-based pigment, often referred to simply high- and/or low-purity iron oxide pigments.

Declarations

Conflict of interest The authors declare that they have no known competing financial interests or personal relationships that could have appeared to influence the work reported in this paper.

References

1. Gettens RJ, Stout GL (1942) Painting materials: a short encyclopaedia. D. Van Nostrand Company, New York
2. Watts I (2010) The pigments from pinnacle point cave 13B, Western Cape, South Africa. J Hum Evol 59:392–411. https://doi.org/10.1016/j.jhevol.2010.07.006
3. Siddall R (2018) Mineral pigments in archaeology: their analysis and the range of available materials. Minerals 8:201. https://doi.org/10.3390/min8050201
4. Kim EK (2012) The meaning of vermilion from tumulus in three Kingdoms' period. Yongnam Archaeol Rev YONGNAM KOGO-HAK 61:51–74
5. Kawano M, Minami T, Tateishi T, Shoda S, Imazu S (2014) Review on the archaeological studies on red pigment in Japan. J Kor Field Archaeol 21:103–121
6. Hradil D, Grygar T, Hradilová J, Bezdička P (2003) Clay and iron oxide pigments in the history of painting. App Clay Sci 22:223–236. https://doi.org/10.1016/S0169-1317(03)00076-0
7. Domingo I, García-Borja P, Roldán C (2012) Identification, processing and use of red pigments (hematite and cinnabar) in the Valencian early Neolithic (Spain). Archaeometry 54:868–892. https://doi.org/10.1111/j.1475-4754.2011.00650.x
8. Lage MCSM, Cavalcante LCD, Klingelhöfer G, Fabris JD (2016) In-situ 57Fe Mössbauer characterization of iron oxides in pigments of a rupestrian painting from the Serra da Capivara National Park, in Brazil, with the backscattering Mössbauer spectrometer MIMOS II. Hyperfine Interact 237:49. https://doi.org/10.1007/s10751-016-1298-1
9. Herrera LK, Cotte M, Jimenez de Haro MC, Duran A, Justo A, Perez-Rodriguez JL (2008) Characterization of iron oxide-based pigments by synchrotron-based micro X-ray diffraction. App Clay Sci 42:57–62. https://doi.org/10.1016/j.clay.2008.01.021
10. Hoffman DL, Angelucci DE, Villaverde V, Zapata J, Zilhão J (2018) Symbolic use of marine shells and mineral pigments by Iberian Neandertals 115,000 years ago. Sci Adv 4:5255. https://doi.org/10.1126/sciadv.aar5255
11. Hoffman DL, Standish CD, García-Diez M, Pettitt PB, Milton JA, Zilhão J, Alcolea-González JJ, Cantalejo-Duarte P, Collado H, De Balbín R, Lorblanchet M, Ramos-Munoz J, Weniger G-Ch, Pike AWG (2018) U-Th dating of carbonate crusts reveals Neandertal origin of Iberian cave art. Science 359:912–915. https://doi.org/10.1126/science.aap7778
12. Martí AP, Zilhão J, d'Errico F, Cantalejo-Duarte P, Domínguez-Bella S, Fullola JM, Weniger GC, Ramos-Muñoz J (2021) The symbolic role of the underground world among Middle Paleolithic Neanderthals. Proc Natl Acad Sci U S A 118:e2021495118. https://doi.org/10.1073/pnas.2021495118
13. Pomiès MP, Menu M, Vignaud C (1999) Red Palaeolithic pigments: natural hematite or heated goethite? Archaeometry 41:275–285. https://doi.org/10.1111/j.1475-4754.1999.tb00983.x
14. Nurdini N, Ilmi MM, Maryanti E, Setiawan P, Kadja GTM (2022) Thermally-induced color transformation of hematite: insight into the prehistoric natural pigment preparation. Heliyon 8:e10377. https://doi.org/10.1016/j.heliyon.2022.e10377
15. Castagnotto E, Locardi F, Slimani S, Peddis D, Gaggero L, Ferretti M (2021) Characterization of the Caput Mortuum purple hematite pigment and synthesis of a modern analogue. Dyes Pigments 185:108881. https://doi.org/10.1016/j.dyepig.2020.108881
16. Han WR, Kim SJ, Moon DH, Park JY (2022) Study on the analysis of red pigments excavated in gaya cultural circle. Conserv Sci Stud 43:45–59
17. Lee HS, Lee HH, Lee KM, Han KS (2014) Study on the manufacturing technology of mural tomb in Goa-Dong of daegaya period. J Conserv Sci 30:457–466. https://doi.org/10.12654/JCS.2014.30.4.14
18. Jang EH, Ahn BC (1999) Red pigment used on the piece of textile excavated from tomb no. 11 of Kyodong in Changyong. Conserv Sci Mueseum 1:87–91. https://doi.org/10.22790/conservation.1999.1.0087
19. Lerf A, Wagner FE, Dreher M, Espejo T, Pérez-Rodríguez JL (2021) Mössbauer study of iron gall inks on historical documents. Herit Sci 9:49. https://doi.org/10.1186/s40494-021-00522-3
20. Tsatskin A, Gendler TS (2016) Identification of "red ochre" in soil at Kfar HaHoresh Neolithic site, Israel: magnetic measurements coupled with materials characterization. J Archaeol Sci Rep 6:284–292. https://doi.org/10.1016/j.jasrep.2016.02.027
21. Novakova AA, Denisov VO, Boeva NM, Tsatskin A (2020) Study of the argillaceous soil and late stone age ceramics made of It.

Crystallogr Rep 65:376–380. https://doi.org/10.1134/S1063774520030232

22. Lee MH, Han MS, Uhm YR, Kim CS (2021) Phase analysis of iron oxides forming the red pigment layer of the ancient earthenwares excavated from the southern Korean Peninsula. J Radioanal Nucl Chem 330:529–538. https://doi.org/10.1007/s10967-021-07866-x

23. Murad E (1988) Properties and behavior of iron oxides as determined by Mössbauer spectroscopy. In: Stucki JW, Goodman BA, Schwertmann U (eds) Iron in soils and clay minerals. Springer, Dordrecht. https://doi.org/10.1007/BF02351598

24. Murad E (1989) Poorly-crystalline minerals and complex mineral assemblages. Hyperfine Interact 47:33–53. https://doi.org/10.1007/BF02351598

25. Cao X, Prozorov R, Koltypin Yu, Kataby G, Felner I, Gedanken A (1997) Synthesis of pure amorphous Fe_2O_3. J Mter Res 12:02–406. https://doi.org/10.1557/JMR.1997.0058

26. Mashlan M, Zboril R, Machala L, Vujtek M, Walla J, Nomura K (2004) Mössbauer spectroscopy in study of thermally induced crystallization of amorphous Fe_2O_3 nanoparticles. J Metastab Nanocryst Mater 20–21:641–647. https://doi.org/10.4028/www.scientific.net/JMNM.20-21.641

27. Ayyub P, Multani M, Barma M, Palkar VR, Vijayaraghavan R (1988) Size-induced structural phase transitions and hyperfine properties of microcrystalline Fe_2O_3. J Phys C Solid State Phys 21:2229–2245

28. Hansen MF, Koch CB, Mørup S (2000) Magnetic dynamics of weakly and strongly interacting hematite nanoparticles. Phys Rev B Condens Matter 62:1124–1135. https://doi.org/10.1103/PhysRevB.62.1124

29. Bødker F, Hansen MF, Koch CB, Lefmann K, Mørup S (2000) Magnetic properties of hematite nanoparticles. Phys Rev B Condens Matter 61:6826–6838. https://doi.org/10.1103/PhysRevB.61.6826

30. Bødker F, Mørup S (2000) Size dependence of the properties of hematite nanoparticles. Europhys Lett 52:217–223. https://doi.org/10.1209/epl/i2000-00426-2

31. Kuhn LT, Lefmann K, Bahl CRH, Ancona SN, Lindgård PA, Frandsen C, Madsen DE, Mørup S (2006) Neutron study of magnetic excitations in 8-nm α-Fe_2O_3 nanoparticles. Phys Rev B Condens Matter 74:184406. https://doi.org/10.1103/PhysRevB.74.184406

32. Murad E, Fabris JD (2010) Kaolin mining and beneficiation: the role of iron. J Phys Conf Ser 217:012066. https://doi.org/10.1088/1742-6596/217/1/012066

33. Heller-Kallai L, Rozenson I (1981) The use of mössbauer spectroscopy of iron in clay mineralogy. Phys Chem Miner 7:223–238. https://doi.org/10.1007/BF00311893

34. Drits VA, Dainyak LG, Muller F, Besson G, Manceau A (1997) Isomorphous cation distribution in celadonites, glauconites and fe-illites determined by infrared, moessbauer and EXAFS spectroscopies. Clay Miner 32:153–179

35. Smyth JR, Dyar MD, May HM, Bricker OP, Acker JG (1997) Crystal structure refinement and mössbauer spectroscopy of an ordered. Triclinic Clinochlore Clays Clay Miner 45:544–550. https://doi.org/10.1346/CCMN.1997.0450406

36. Kodama H, Longworth G, Townsend MG (1982) A Mössbauer investigation of some chlorites and their oxidation products. Can Mineral 20:585–592

37. Memon M, Memon KS, Akhtar MS, Stüben D (2009) Characterization and quantification of iron oxides occurring in low concentration in soils. Commun Soil Sci Plant Anal 40:162–178. https://doi.org/10.1080/00103620802649005

38. De Grave E, Bowen LH, Vochten R, Vandenberghe RE (1988) The effect of crystallinity and Al substitution on the magnetic structure and morin transition in hematite. J Magn Magn Mat 72:141–151. https://doi.org/10.1016/0304-8853(88)90182-5

39. Schwertmann U, Taylor RM (1989) In: Dixon JB, Weed SB (eds) Minerals in soil environments. Soil Sci. Soc. Am., Madison, new Edn in the press

40. Maher B, Taylor R (1988) Formation of ultrafine-grained magnetite in soils. Nature 336:368–370. https://doi.org/10.1038/336368a0

41. Vodyanitskii YN (2013) Biogeochemical role of magnetite in urban soils. Eurasian Soil Sci 46:317–324. https://doi.org/10.1134/S1064229313030137

42. Fouad DE, Zhang C, El-Didamony H, Yingnan L, Mekuria TD, Shah AH (2019) Improved size, morphology and crystallinity of hematite (α-Fe_2O_3) nanoparticles synthesized via the precipitation route using ferric sulfate precursor. Results Phys 12:1253–1261. https://doi.org/10.1016/j.rinp.2019.01.005

43. De Faria DLA, Venâncio Silva S, De Oliveira MT (1997) Raman microspectroscopy of some iron oxides and oxyhydroxides. J Raman Spectrosc 28:873–878. https://doi.org/10.1002/(SICI)1097-4555(199711)28:11%3c873::AID-JRS177%3e3.0.CO;2-B

44. Hanesch M (2009) Raman spectroscopy of iron oxides and (oxy) hydroxides at low laser power and possible applications in environmental magnetic studies. Geophys J Int 177:941–948. https://doi.org/10.1111/j.1365-246X.2009.04122.x

45. Rull F, Martinez-Frias J, Sansano A, Medina J, Edwards HGM (2004) Comparative micro-Raman study of the Nakhla and Vaca Muerta meteorites. J Raman Spectrosc 35:497–503. https://doi.org/10.1002/jrs.1177

46. Fouad NE, Ismail HM, Zaki MI (1998) Recovery of red iron oxide pigmentary powders from chemically modified steel-plickling chemical waste. J Mater Sci Lett 17:27–29. https://doi.org/10.1023/A:1006533405891

47. Cornell RM, Schwertmann U (2003) The iron oxide: structures, properties, reactions, occurrences and uses, 2nd edn. Wiley-VHC, Weinheim

48. Singh B, Wilson M, McHardy W, Fraser A, Merrington G (1999) Mineralogy and chemistry of ochre sediments from an acid mine drainage near a disused mine in Cornwall, UK. Clay Miner 34:301–317. https://doi.org/10.1180/000985599546172